



Silver nanoparticles produced via a green synthesis using the rhamnolipid as a reducing agent and stabilizer

L. I. Bazylyak¹ · A. R. Kytsya^{1,2} · P. Y. Lyutyi^{2,3} · N. I. Korets'ka¹ · Ya. V. Pilyuk¹ · O. I. Kuntiyi³

Received: 17 February 2022 / Accepted: 14 December 2022 / Published online: 7 January 2023
© King Abdulaziz City for Science and Technology 2022

Abstract

Silver nanoparticles (AgNPs) stabilized by rhamnolipid (RL), which was separated from the supernatant of the genus *Pseudomonas* sp. PS-17, were synthesized. Using TEM it was found that the mean size of obtained AgNPs does not depend on the initial concentration of Ag⁺ but is increased with the decrease of the concentration of RL. During XRD-phase analysis it was determined, that the Ag (space group *Fm-3m*, Cu-structure type) is the main phase that was identified. The kinetics of the formation of AgNPs was studied in detail using the UV–Vis spectroscopy. It was observed that in all cases the kinetic curves are sigmoidal shape and are characterized by a well-notable induction period that permits to assume the homogeneous nucleation of AgNPs and their autocatalytic growth. Experimental kinetic curves were fitted using different types of Finke-Watzky schemes of continuous nucleation and fast autocatalytic growth of particles and the observable rate constants of nucleation and growth were estimated. Based on the established regularities of “green” synthesis of AgNPs stabilized by RL, the method of obtaining their colloidal solutions was optimized. A laboratory model of a flow tubular reactor for the synthesis of colloidal solutions of AgNPs has been created.

Keywords Green synthesis · Silver nanoparticles · Rhamnolipid · Kinetics · Flow tubular reactor

Introduction

Silver nanoparticles (AgNPs) have great potential in a broad range of applications as antimicrobial agents (Kuntiyi et al. 2021a, b), biomedical device coatings (Grytsenko et al. 2018), drug-delivery carriers, imaging probes, diagnostic and optoelectronic platforms (Lee and Jun 2019), since they have discrete physical, chemical and optical properties and biochemical functionality. Silver nanoparticles have been investigated extensively due to their superior physical,

chemical, and biological characteristics, and their superiority stems mainly from the size, shape, composition, crystallinity and structure of AgNPs compared to their bulk forms (Syafuddin et al. 2017; Kumar et al. 2008; Desireddy et al. 2013; Sun et al. 2002; Atwater et al. 2010; Koval'chuk et al. 2010). Recently in the literature, there have been reports of the AgNPs obtaining in different biological solutions via the so-called “green methods”, for example, using plant extract (Krishnaraj et al. 2010; Vilchis-Nestor et al. 2008; Chandran et al. 2006; Amooaghaie et al. 2015; Bar et al. 2009; Some et al. 2018; Ahmad et al. 2019; Mousavi et al. 2018; Srikar et al. 2016) and supernatants obtained from bacterial (Płaza et al. 2016; Gurunathan et al. 2009; Shahverdi et al. 2007; Kalishwaralal et al. 2008; Nanda et al. 2009; Kuntiyi et al. 2020) or fungus cultures (Vigneshwaran et al. 2007; Bhainsa et al. 2006; Kapoor et al. 2021). In this green chemistry approach, several bacteria, including *Pseudomonas stutzeri* AG259 (Klaus et al. 1999), *Lactobacillus* (Nair et al. 2002), *Bacillus licheniformis* (Kalimuthu et al. 2008), *Escherichia coli* (Gurunathan et al. 2009), *Brevibacterium casei* (Kalishwaralal et al. 2020), plant extracts such as *Allophylus cobbe* (Gurunathan et al. 2014a, b), *Artemisia princeps* (Gurunathan et al. 2015), *Typha angustifolia* (Gurunathan et al.

✉ L. I. Bazylyak
bazylyak.L.I@nas.gov.ua

¹ Department of Physical Chemistry of Fossil Fuels of the Institute of Physical–Organic Chemistry and Coal Chemistry named after L. M. Lytvynenko of the National Academy of Sciences of Ukraine, 3a Naukova Str., Lviv 79060, Ukraine

² Karpenko Physico-Mechanical Institute of the National Academy of Sciences of Ukraine, 5 Naukova Str., Lviv 79060, Ukraine

³ Lviv Polytechnic National University, 12 Bandery Str., Lviv 79013, Ukraine

2015) were used. In addition to these, several biomolecules, such as biopolymers (Leung et al. 2010), starch (Kumar et al. 2014), fibrinolytic enzyme (Deepak et al. 2011), and aminoacids (Shankar and Rhim 2015) were used. Biological entities could act simultaneously as reducing and stabilizing agents. Increasing attention to the biological synthesis of AgNPs can be attributed to environmental and economic reasons. Green synthesis of AgNPs with naturally occurring reducing agents could be a promising method to replace more complex physiochemical syntheses since green synthesis is free from toxic chemicals and hazardous byproducts and instead involves natural capping agents for the stabilization of AgNPs. Use of biological agents seems to provide controlled particle size and shape, which is an important factor for various biomedical applications (Gurunathan et al. 2014a, b). The other advantages of biological agents are the availability of a vast array of biological resources, a decreased time requirement, high density, stability, and the ready solubility of prepared nanoparticles in water. Biogenic surfactants are one of the promising agents for the development of nanocomposites, they are ecologically safe alternative to toxic chemicals. The most known biosurfactants are rhamnolipids, which represent by themselves the low molecular weight secondary metabolites of bacteria genera *Pseudomonas*.

In the previous article (Bazylak et al. 2022) we reported about high antimicrobial activity of AgNPs stabilized by RL against some test microorganisms such as *Escherichia coli*, *Staphylococcus aureus*, *Pseudomonas aeruginosa*, *Mycrococcus luteus* (human pathogenes) and *Agrobacterium tumefaciens* and *Xanthomonas campestris* (phytopathogenes). It was established, that the values of minimum bactericidal concentration (MBC) of AgNPs for the *A. tumefaciens*, *X. campestris* and *M. luteus* are very low and are equal to 1.5 µg/mL. Therefore, the low values of MBC compared to the low cost of obtained “AgNPs-RL” solutions make them attractive in terms of the development of antimicrobial drugs with a broad spectrum of action. That is why the main aim of the presented work was to synthesize the AgNPs in the presence of rhamnolipid, to investigate in detail the kinetics and mechanism of the AgNPs formation via the reduction of Ag⁺ by RL as well as to investigate the influence of experimental conditions on the properties of obtained nanoparticles to design the method of continuous synthesis of “AgNPs-RL” solutions.

Experimental details

Synthesis of AgNPs

The rhamnolipid of natural origin (RL), which represents by itself the product of microbial synthesis of the strain

Pseudomonas sp. PS-17 was used as the reducing agent and stabilizer for the “green” synthesis of AgNPs. RL was separated accordingly to described earlier technique (Pokynbroda et al. 2019; Yerokhin et al. 2006; Karpenko et al. 2009) and was provided for the investigations by the scientific group led by professor Olena Karpenko (Department of Physical Chemistry of Fossil Fuels of the Institute of Physical-Organic Chemistry and Coal Chemistry named after L. M. Lytvynenko of the National Academy of Sciences of Ukraine). The structural formula of the RL is presented in Fig. S-1 (Supplemental Information). As it can be seen from this formula, the RL contains carboxyl and two sugar (rhamnose) functional groups as well as long hydrocarbon chains. Therefore, it can simultaneously act as a ligand for silver ions, a reducing agent of Ag⁺ ions, as well as a surface-active substance, that is, a stabilizer of AgNPs.

In accordance with the typical synthesis 95 mL of a solution of RL was added into a two-necked flask equipped with a magnetic stirrer and Dimroth-type condenser and placed into the thermostat. pH of the RL solution was regulated by NaOH (titrant, Kharkovreachem, Ukraine) and was controlled using the Adwa AD1000 pH/mV and Temperature meter (Adwa Instruments, Hungary). After reaching the operative temperature, 5 mL of AgNO₃ (Aldrich, > 99.0%) solution of a given concentration was added into the flask.

Kinetics of the reaction was monitored via the change of UV–Vis spectra of the working solution applying the UVmini-1240 spectrophotometer (Shimadzu, Japan) with the use of 1 cm cuvette at a wavelength range from 300 to 1100 nm. The COPASI Software (Hoops et al. 2006) was used for the evaluation of the observable rate constants of the process.

The completeness of the reaction conversion was tested using the hydrazine test: after the finishing of the kinetic measurements the 0.05 mL of hydrazine hydrate (N₂H₄·H₂O, Systema Optimum, Ukraine, > 98.0%) was added to 5 mL of the solution, and UV–Vis spectrum of the sample was recorded. It should be noted, that in all of the investigated experimental conditions any changes in the spectra before and after hydrazine addition were not observed. This fact proves the near 100% degree of reduction of Ag⁺ to Ag⁰.

Characterisation of AgNPs

Obtained AgNPs were characterized using transmission electron microscopy (TEM) and X-ray diffraction analysis (XRD). TEM images of obtained AgNPs were recorded using the JEM-I230 (JEOL, Japan). The size of AgNPs was evaluated using AxioVision V 4.8.2.0 (Carl Zeiss Microscopy) software. The samples for TEM investigations were prepared by application of micro-drops (~0.5 µL) of silver sol on the carbon grid with the subsequent drying under the ambient conditions.

The samples for the XRD measurements were prepared by concentrating the AgNPs solution at 80 °C with the subsequent precipitation of AgNPs by ethanol (96%), decantation of the precipitate and the following drying under the ambient conditions.

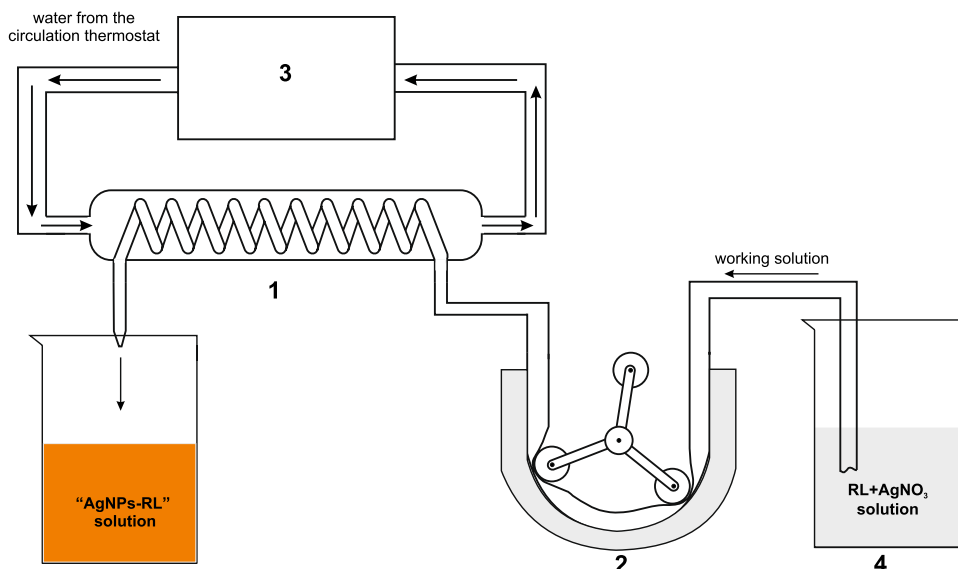
X-ray powder diffraction data were obtained with the use of the X-ray diffractometer (Aeris-Malvern Panalytical) with Cu-K α radiation operated at a voltage of 40 kV, a current of 15 mA and setup, beam knife high, start angle 25° (2 θ), end angle 100°, step size 0.0217.

XRD-phase analysis was performed using the Highscore software and referenced with the International Center for Diffraction Data (ICDD). All procedures including the indexing, structure solutions and the refinement of profile and structural parameters were performed with the WinCSD (Akselrud and Grin 2014) program package.

The scheme of the laboratory plug flow reactor for the AgNPs synthesis

The constructed laboratory setup for the synthesis of AgNPs consisted of the thermostated serpentine reactor (1) connected to the peristaltic pump (2) and circulation thermostat (3) (Fig. 1). Inner pipe diameter was 4 mm and the pipe length was 800 mm; the total volume of a reactor was 10 mL. The working solution (4) (RL + AgNO₃) was fed into the reactor with the given rate, providing the complete reduction of Ag⁺ to Ag⁰.

Fig. 1 The scheme of the laboratory setup for the continuous synthesis of AgNPs



Results and discussion

Kinetics of “green” synthesis of AgNPs

An influence of the synthesis conditions on the kinetics of Ag⁺ reduction by RL was studied in detail to optimize the method of obtaining the AgNPs solutions. The kinetics has been studied using UV–Vis spectroscopy via the change of the maximum absorbance band of the surface plasmon resonance (SPR) of AgNPs (Sandoe et al. 2019; Kytsya et al. 2019).

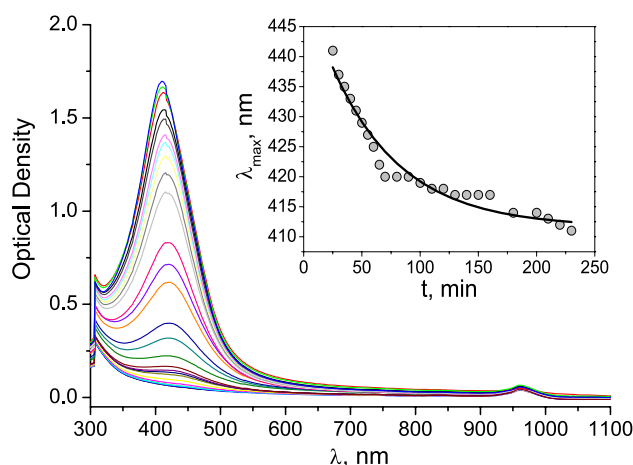


Fig. 2 The evolution of the spectra of working solution during the synthesis of AgNPs at pH 8. Insertion is the changing of the maximum of SPR during the synthesis

An influence of pH on the kinetic parameters of AgNPs formation

An influence of pH on the kinetics of AgNPs formation was studied at 70 °C (Fig. 2). The initial concentrations of Ag^+ and RL were 2×10^{-4} mol/L and 4 g/L, respectively.

It was found that the spectra of the solutions are characterized by a clear absorption maximum which may indicate the spherical shape of the obtained AgNPs. At the same time, during the synthesis a shift of the absorption maximum in the short-wavelength region was observed (Fig. 2, insertion). This phenomenon can be explained as follows. The position of the SPR band is significantly influenced by the value of the dielectric constant of the medium (Slistan-Grijalva et al. 2005; Kytsya et al. 2014) and in the case of surfactants that are adsorbed on the particle surface—by the interaction between surfactant molecules and surface atoms of the growing silver particle. With increasing the particle size during the synthesis, the ratio of surface atoms that interact with the surfactant molecules is decreased, which, accordingly, affects the position of the SPR band of the AgNPs solution. Since the ratio of the values of the current and the final optical density of the solution is proportional to the conversion of the reaction $a = \text{O.D.}_t / \text{O.D.}_{\text{max}}$ (Sandoe et al. 2019), the obtained spectra were used for the plotting of the kinetic curves of the processes (Fig. 3). As it can be seen from Fig. 3a, the kinetic curves of the AgNPs formation are sigmoidal which indicates on the autocatalytic nature of the process. From the obtained kinetic curves the time of the induction period (t_{ind}) and the maximal rate of the process (da/dt) were calculated (Table 1).

Kinetic curves (Fig. 3a) indicate a significant effect of pH of the reaction mixture on the rate of the formation of AgNPs. However, the rate of nucleation of AgNPs ($1/t_{\text{ind}}$) is proportional to the pH of the reaction medium (Fig. 3b). At

Table 1 Dependence of the kinetic parameters of the AgNPs formation on reaction conditions

pH	$[\text{Ag}^+]_0 \cdot 10^3$, mol/L	C (RL), g/L	t , °C	t_{ind} , min	da/dt , min^{-1}
8	0.2	4	70	45	0.008
9				7	0.054
11				3	0.09
10	0.2	4	70	5.0	0.08
	0.5			3.3	0.13
	1			1.8	0.25
10	0.2	1	70	9	0.04
		2		7	0.06
10	0.2	4	50	∞	0
			60	40	0.01
			80	2.5	0.14

the same time, the dependence of the rate AgNPs growth on pH is nonmonotonic. Thus, based on the obtained data, we can assume that the optimal pH for the synthesis of AgNPs stabilized by RL is pH 10 due to the following reasons. As can be seen from the data presented in Table 1, the increase of pH from 10 to 11 leads to an insufficient decrease in the induction period as well as the rate of growth of AgNPs. However, the increase in pH causes the contamination of the final product by NaOH by an order of magnitude. Therefore, all subsequent studies were performed at pH 10.

An influence of initial concentrations of RL and AgNO_3 on the kinetics of the AgNPs formation

The dependence of the kinetics of AgNPs formation on the initial concentrations of RL and AgNO_3 were studied at 70 °C and pH 10.

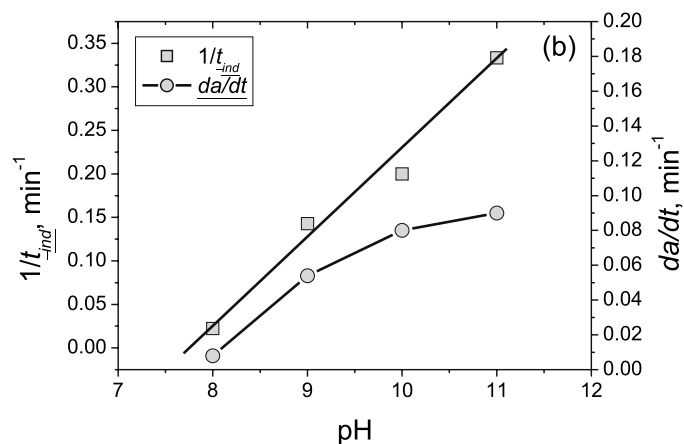
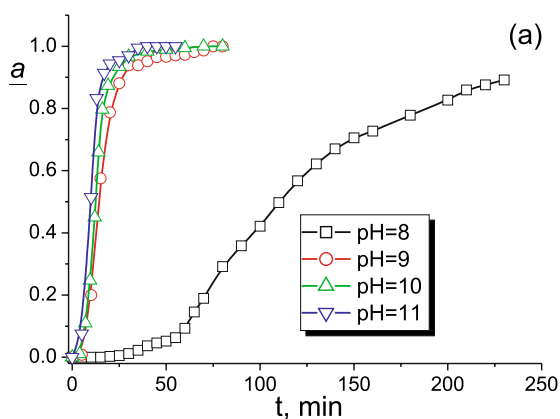


Fig. 3 The kinetic curves of AgNPs formation at different pH (a) and the dependencies of the rates of nucleation and growth of AgNPs on pH (b)

It was found that in the all of cases the nature of the evolution of absorption spectra during the synthesis of AgNPs is similar to the described above, namely in all cases an increase of the absorption intensity over time and a shift of the SPR band in the shortwave region were observed. Based on the obtained spectra the kinetic curves of AgNPs were plotted (Fig. 4) and the kinetic parameters of the process were determined (Table 1).

It was found that both the nucleation rate and the growth rate of AgNPs linearly depend on the initial concentration of rhamnolipid (RL) (Fig. 5a). Thus, due to the fact that the concentration of rhamnolipid in the reaction mixture is much higher compared to the concentration of Ag^+ , we can assume the first order of the processes of nucleation and growth of AgNPs in respect to RL. At the same time, the dependencies of the nucleation rates and growth of AgNPs on the initial concentration of silver ions are close to linear too (Fig. 5b). However, since the concentration of Ag^+ is changed during

the synthesis, as well as due to the autocatalytic nature of the process, such dependences require additional analysis (vide infra, “Analysis of the kinetics of AgNPs formation in RL solutions”).

Activation parameters of the AgNPs formation

To establish the activation parameters of the silver ion reduction with rhamnolipid, the effect of temperature on the kinetics of AgNPs formation was studied under the following synthesis conditions: $[AgNO_3]_0 = 2 \times 10^{-4}$ mol/L, RL = 4 g/L, pH 10.

It was found that at 50 °C the spectra of the working solution does not change during 250 min (Fig. 6a), i.e. the rate of the reduction of silver ions by rhamnolipid at this temperature is extremely slow. Based on the values of the kinetic parameters of the process (Table 1), the activation energies of nucleation and growth of AgNPs were calculated

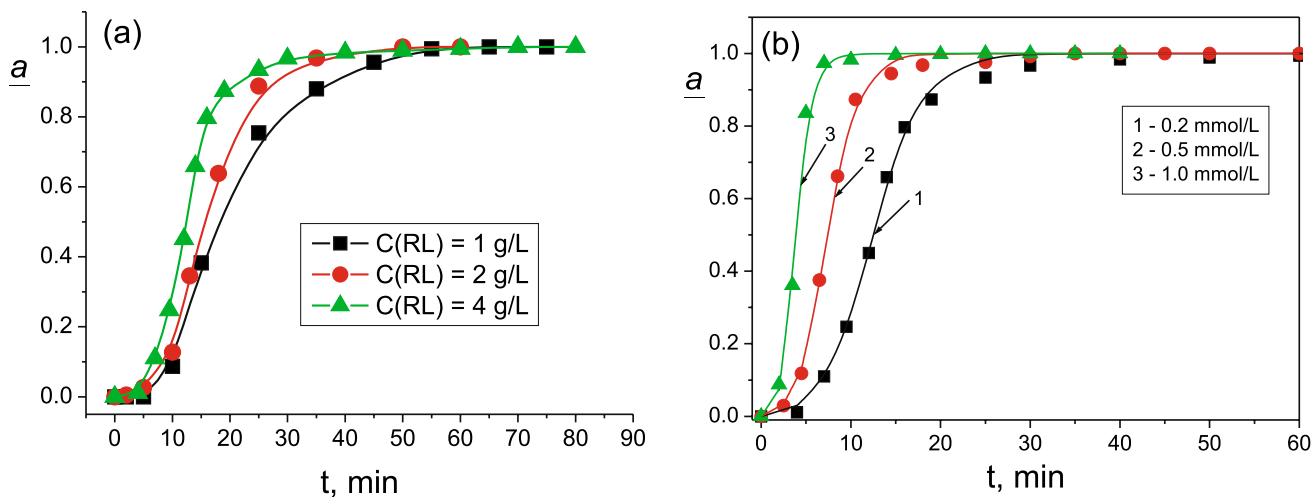


Fig. 4 The kinetic curves of AgNPs formation at different initial concentrations of RL (a) and $AgNO_3$ (b)

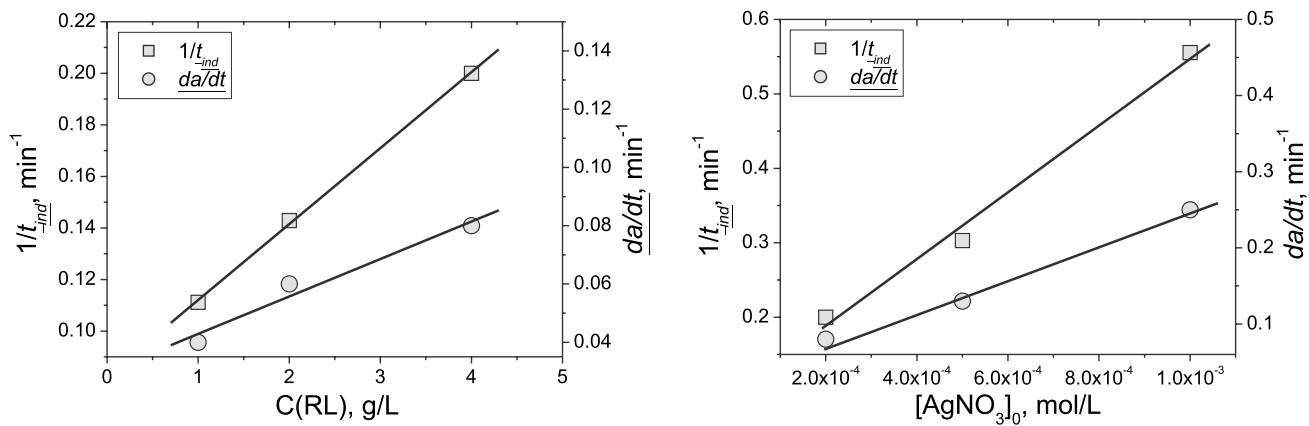


Fig. 5 The dependencies of the rates of nucleation and growth of AgNPs on the initial concentrations of RL (a) and $AgNO_3$ (b)

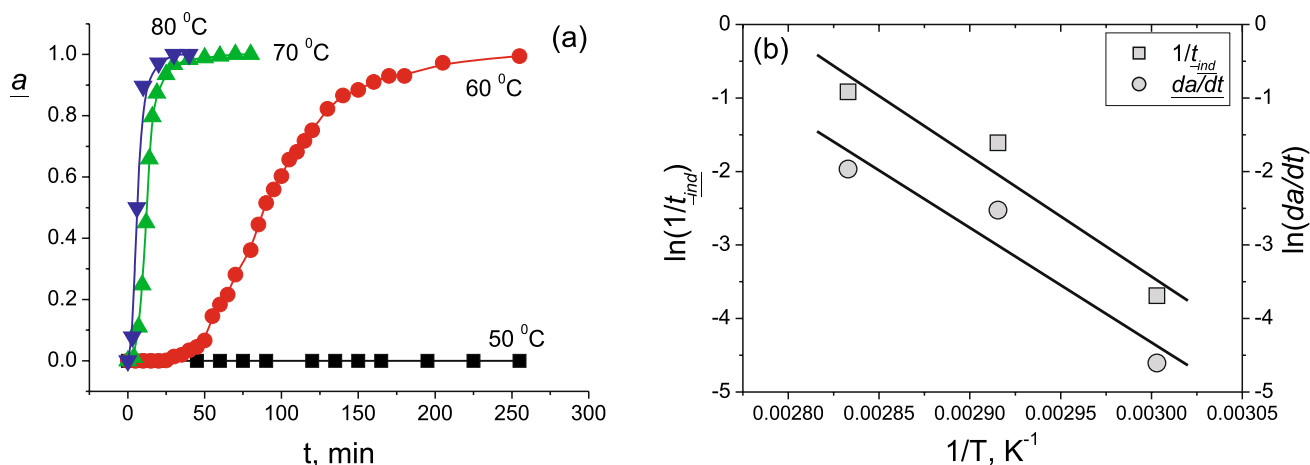


Fig. 6 The kinetic curves of AgNPs formation at different temperatures (a) and the dependencies of the rates of nucleation and growth of AgNPs in Arrhenius coordinates (b)

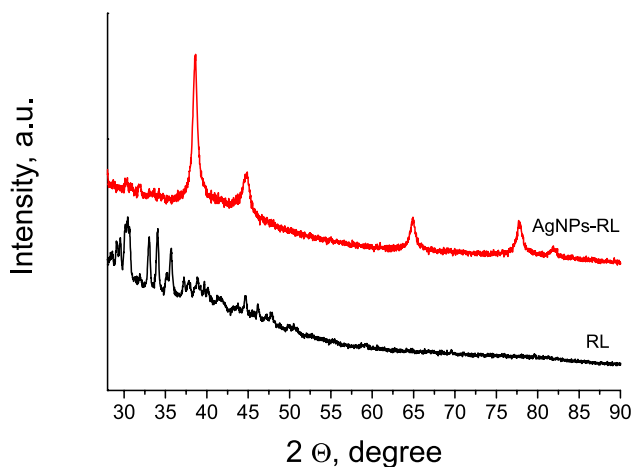


Fig. 7 XRD-pattern of AgNPs stabilized by RL and the scan of RL

(Fig. 6b), which are equal to 135 ± 35 and 140 ± 40 kJ/mol, respectively.

High and almost identical values of activation energies of the nucleation and the growth of silver nanoparticles exclude the diffusion nature of the process of nucleation of a new phase as well as with a high probability indicate the same nature of the chemical processes that occur during the nucleation and growth of AgNPs.

Characterization of AgNPs stabilized by RL

Obtained AgNPs were characterized using the XRD and TEM methods.

During XRD-phase analysis of the obtained sample (Fig. 7) the Ag (space group $Fm-3m$, Cu—structure type) as the main phase was identified and the unknown small peaks in the 2θ range $25-30^\circ$, which do not correspond to

silver as well as to silver oxides were observed. The assumption that these peaks belong to remains of RL was made. To confirmed or disprove this, the XRD scan of RL (Fig. 7) was performed and a good match was found. Graphical representation of the Rietveld refinements of the powder data of the sample is shown on Fig. S-2 (Supplemental Information). Refined lattice cell parameter for Ag is equal to $a = 4.050(1)$ Å.

Using TEM it was found that the obtained AgNPs are polydisperse and mostly irregular in shape (Fig. 8a).

However, a detailed analysis of TEM images obtained at high magnification ($\sim 100,000$) revealed that large nanoparticles (10–40 nm) are surrounded by a “cloud” of small (1–4 nm) particles (Fig. 8, a, insertion). A similar pattern is observed for all studied samples and can be caused by the method of preparation of samples for TEM, namely: for TEM investigations the microdrop of the AgNPs solution was applied on a suitable substrate and dried under the ambient conditions. Thus, the concentration of AgNPs in the microdrop is slowly increased. During the evaporation of water, the fluctuations of the concentrations of small particles could be formed on the inhomogeneities of the substrate and such fluctuations led to the uneven coagulation of small nanoparticles and, respectively, to the formation of large ($\sim 10-40$ nm) particles of irregular shape. Based on the TEM-images the histograms of the particle size distribution (PSD) were plotted (Figs. 8b, Figs. S3–S6, see Supplemental Information). Presented PSD histograms are based on the analysis of 3 to 6 TEM-images (120–150 particles) for each of the conditions of the experiment. The mean size and polydispersity of AgNPs were calculated using the Gaussian function.

It was found (Fig. 8b and Table 2) that the fractions of particles of 1–4 nm in size are more than 70% for the $C(RL) = 4$ g/L. At the same time, the distribution of large

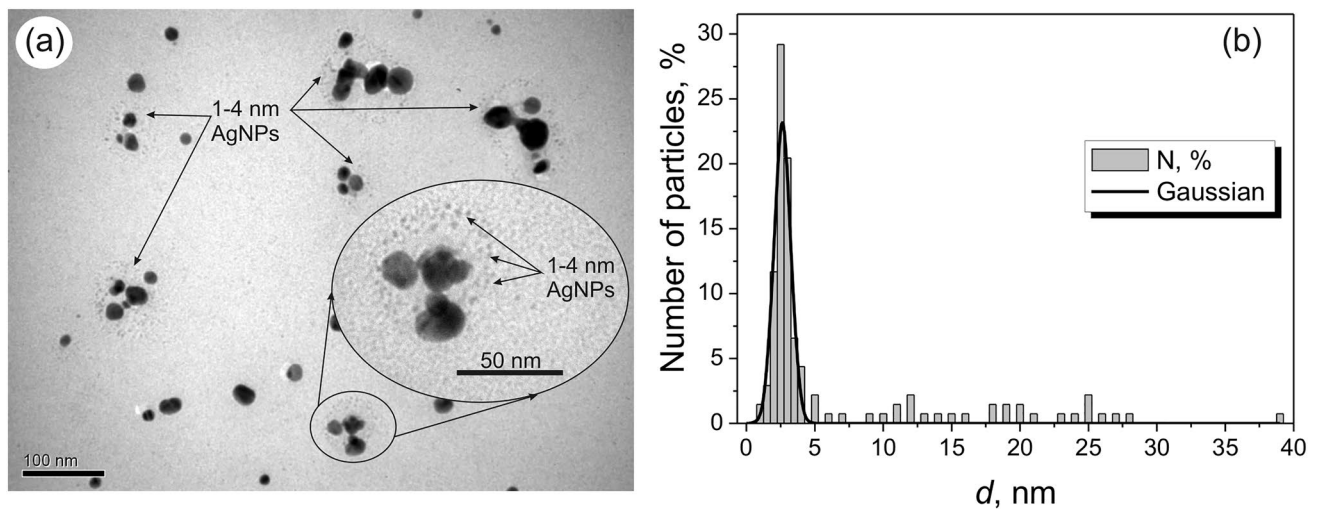


Fig. 8 TEM-image and histogram of the particle size distribution of AgNPs obtained at 70 °C and initial concentrations of RL and AgNO₃ equal to 4 g/L and 1×10^{-3} mol/L, respectively

Table 2 Dependency of the size of obtained AgNPs on the reaction conditions

[Ag ⁺] ₀ · 10 ³ , mol/L	C(RL), g/L	$d \pm \Delta d$, nm	The fraction of particles with a size within 1–4 nm, %
0.2	4	2.6 ± 1.4	70
0.5		2.6 ± 1.3	70
1		2.6 ± 1.2	75
0.2	1	4.8 ± 4.3	40
	2	2.6 ± 2.2	60

(above 10 nm) particles is nonmonotonic and cannot be described even using polymodal distribution functions. These facts indirectly confirm the above-mentioned assumption about the coagulation of particles during the preparation of the sample for TEM investigations, because, in the case of coagulation of AgNPs at the stage of their growth the distribution of the obtained AgNPs should be more monotonous and PSD should be described by the Gaussian function.

As it can be seen from the presented in Table 2 data, an increase in the concentration of silver ions has almost no effect on the size of the resulting AgNPs: the values of their average diameter (d) and polydispersity (Δd) are close. At the same time, with the decrease of the RL concentration to 2 g/L, an increase of Δd AgNPs is observed, and with a further decrease of the stabilizer concentration, together with Δd , the value of the average particle diameter is also increased.

Analysis of the kinetics of AgNPs formation in RL solutions.

Based on the obtained experimental data the following generalizations and assumptions which are necessary for further analysis of the mechanism of formation of AgNPs in RL solutions can be done:

- i) the kinetic curve of AgNPs formation is characterized by a pronounced induction period and is sigmoidal which indicates, that the reduction of Ag⁺ in RL solutions is autocatalytic process;
- ii) the order of reaction with respect to RL is equal to 1; therefore, given that the concentration of RL in the solution in the all of cases is much higher than the concentration of silver ions, the “gross reaction” of the formation of AgNPs can be represented as Ag⁺ → Ag⁰;
- iii) due to the high activation energy of the nucleation and the growth the diffusion nature of the process of nucleation of AgNPs is unlikely, i.e. the limiting stages of nucleation and growth are the chemical processes of reduction of silver ions in solution (nucleation) or on the surface of AgNPs (growth);

Therefore, the kinetic curves of AgNPs formation in rhamnolipid solutions were analyzed using the different Finke-Watzky schemes, namely (1) FW-2 (Watzky and Finke. 1997), (2) FW-3 (Widegren et al. 2001), (3) FW-4 (Besson et al. 2005) and (4) FW-4a (Finney and Finke. 2008; Finney et al. 2012; Özkar and Finke. 2016):



Here A is a precursor, B is a metal atom in the nanoparticle and C is a metal atom in the agglomerated nanoparticle.

The systems of ordinary differential equations (ODE) for such schemes are written as follows:

$$\begin{aligned} \frac{dA}{dt} &= -k_{1,obs}A - k_gAB \\ \frac{dB}{dt} &= k_{1,obs}A + k_gAB \end{aligned} \quad (5)$$

$$\begin{aligned} \frac{dA}{dt} &= -k_{1,obs}A - k_gAB \\ \frac{dB}{dt} &= k_{1,obs}A + k_gAB - 2k_3B^2 \\ \frac{dC}{dt} &= k_3B^2 \end{aligned} \quad (6)$$

$$\begin{aligned} \frac{dA}{dt} &= -k_{1,obs}A - k_gAB \\ \frac{dB}{dt} &= k_{1,obs}A + k_gAB - 2k_3B^2 - k_4BC \\ \frac{dC}{dt} &= k_3B^2 + 0.5k_4BC \end{aligned} \quad (7)$$

$$\begin{aligned} \frac{dA}{dt} &= -k_{1,obs}A - k_gAB - k_4AC \\ \frac{dB}{dt} &= k_{1,obs}A + k_gAB - 2k_3B^2 \\ \frac{dC}{dt} &= k_3B^2 + 0.5k_4AC \end{aligned} \quad (8)$$

The **FW-2** scheme is usually used to describe the kinetics of the metal nanoparticles formation in solutions in the absence of the agglomeration of particles. At the same time, the schemes **FW-3**, **FW-4** and **FW-4a** take into account the processes of the nanoparticle aggregation (6), secondary agglomeration of particles (7), as well as the autocatalytic growth of agglomerates (8). In Table 3 there are observed rate constants of the corresponding reactions obtained by optimization of the experimental kinetic curves.

It was found that at a concentration of RL equal to 4 g/L the kinetic curves are satisfactorily described by the scheme **FW-2**. As it can be seen from the presented in Table 3 data, calculated according to the schemes **FW-2** and **FW-3** values of $k_{1,obs}$ and k_g almost coincide in the range of initial concentrations of silver nitrate within 0.0002–0.001 mol/L; the values k_3 are low compared to values k_g and the values of the root mean square deviation (RMS) for the studied cases do not depend on the selected model. Thus, the analysis of the kinetics of AgNPs formation at different initial concentrations of AgNO₃ confirms the above-mentioned assumption about the absence of agglomeration of the particles at the stage of their growth.

However, with the decrease of RL concentration the polydispersity of the obtained particles as well as their average diameter increase (Table 2); i.e., the agglomeration processes in these systems are probable. This assumption is in good agreement with the results of the calculations presented in Table 3. As we can see, the values of RMS are reduced by half in the case of using the **FW-3** scheme for the optimization of kinetic curves of AgNPs formation at different RL concentrations and the lowest values of RMS are observed for the **FW-4a** scheme.

As it can be seen from Fig. 9, the kinetic curves are well described using the scheme **FW-4a**. This means, that the formation of AgNPs at low concentrations of rhamnolipid occurs through the stage of formation of agglomerates of particles with their subsequent autocatalytic growth. It should be noted that the values of the observed rate constants of nucleation, growth, aggregation and secondary autocatalytic growth of AgNPs cannot be directly used to estimate the size and concentration of the obtained nanoparticles due to the pseudo-homogeneous approximation used in all **FW** models. However, it is necessary to pay attention to the values of the rate constants of coagulation (k_3) and the rate constants of secondary autocatalytic growth (k_4) of nanoparticles at RL concentrations of 1 and 2 g/L. The value

Table 3 Calculated values of the observable rate constants of the pseudo-elementary reactions of the AgNPs formation in solutions of rhamnolipid

[Ag ⁺] ₀ , mol/L	[RL], g/L	Parameter	FW-2	FW-3	FW-4	FW-4a
2 × 10 ⁻⁴	4	<i>k</i> _{1,obs} , min ⁻¹	0.0032	0.004	–	–
		<i>k</i> _g , mol ⁻¹ ·L·min ⁻¹	1890	1800	–	–
		<i>k</i> ₃ , mol ⁻¹ ·L·min ⁻¹	–	190	–	–
		<i>k</i> ₄ , mol ⁻¹ ·L·min ⁻¹	–	–	–	–
		RMS	4 × 10 ⁻⁶	4 × 10 ⁻⁶	–	–
		5 × 10 ⁻⁴	4	<i>k</i> _{1,obs} , min ⁻¹	0.006	0.004
<i>k</i> _g , mol ⁻¹ ·L·min ⁻¹	1260			1260	–	–
<i>k</i> ₃ , mol ⁻¹ ·L·min ⁻¹	–			200	–	–
<i>k</i> ₄ , mol ⁻¹ ·L·min ⁻¹	–			–	–	–
RMS	6 × 10 ⁻⁶			6 × 10 ⁻⁶	–	–
10 × 10 ⁻⁴	4			<i>k</i> _{1,obs} , min ⁻¹	0.008	0.007
		<i>k</i> _g , mol ⁻¹ ·L·min ⁻¹	1300	1350	–	–
		<i>k</i> ₃ , mol ⁻¹ ·L·min ⁻¹	–	0.01	–	–
		<i>k</i> ₄ , mol ⁻¹ ·L·min ⁻¹	–	–	–	–
		RMS	1 × 10 ⁻⁵	1 × 10 ⁻⁵	–	–
		2 × 10 ⁻⁴	1	<i>k</i> _{1,obs} , min ⁻¹	0.007	0.0016
<i>k</i> _g , mol ⁻¹ ·L·min ⁻¹	830			1650	1680	1800
<i>k</i> ₃ , mol ⁻¹ ·L·min ⁻¹	–			960	980	2050
<i>k</i> ₄ , mol ⁻¹ ·L·min ⁻¹	–			–	0	540
RMS	8 × 10 ⁻⁶			4 × 10 ⁻⁶	4 × 10 ⁻⁶	3 × 10 ⁻⁶
2	<i>k</i> _{1,obs} , min ⁻¹			0.004	0.0023	0.0023
	<i>k</i> _g , mol ⁻¹ ·L·min ⁻¹		1300	1660	1650	1900
	<i>k</i> ₃ , mol ⁻¹ ·L·min ⁻¹		–	440	430	1500
	<i>k</i> ₄ , mol ⁻¹ ·L·min ⁻¹		–	–	0	1200
	RMS		5 × 10 ⁻⁶	2.6 × 10 ⁻⁶	2.6 × 10 ⁻⁶	2 × 10 ⁻⁶

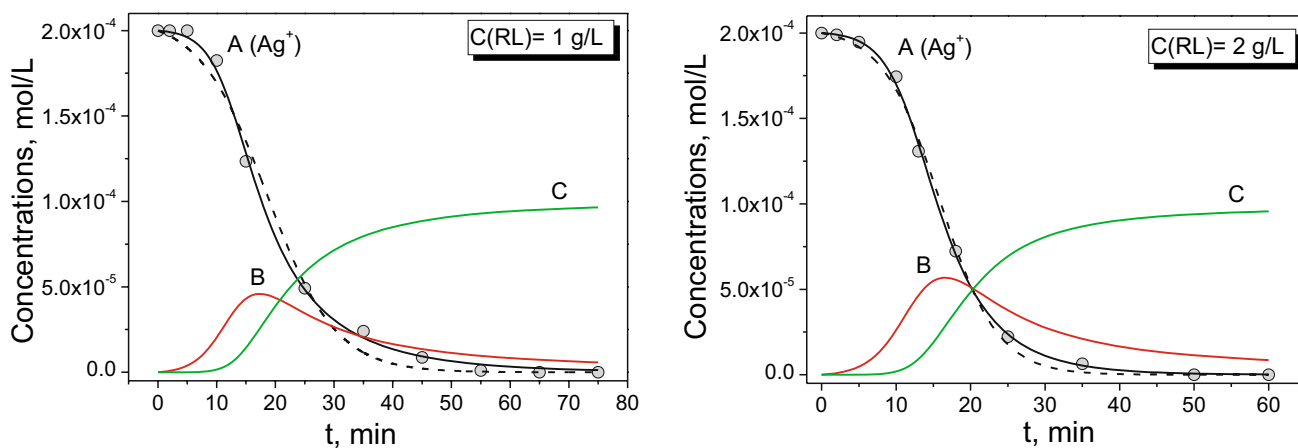


Fig. 9 Calculated by the schemes **FW-2** (dashed line) and **FW-4a** values of concentrations of A, B and C. Points are the experimental data obtained at the different concentrations of RL

of *k*₃ for a low concentration of RL is higher compared to *k*_g and *k*₄, which indicates the predominance of the coagulation processes in the reaction mixture. However, increasing the concentration of RL to 2 g/L leads to a sharp increase in the value of *k*₄ and decreasing *k*₃. Hence, in this case the processes of growth (both primary and secondary) of

particles are predominant. The above considerations are in good agreement with the results of TEM investigations of the obtained AgNPs (Table 2). The decrease of the concentration of RL in the reaction mixture to 2 g/L leads to the increase of the polydispersity of the particles caused by the secondary autocatalytic growth of agglomerates (*k*₄),

but the average diameter of AgNPs does not change. Further decrease of RL concentration up to 1 g/L leads to the fact that the concentration of surfactant in solution becomes insufficient for the effective stabilization of AgNPs and the agglomeration processes (k_3) predominate in the system. Respectively, simultaneously with the increase of polydispersity of AgNPs their average diameter also increases.

Testing of the plug flow reactor for the synthesis of AgNPs

The scheme of the continuous tubular reactor used for the testing of the possibility of production of the “AgNPs-RL” solutions is presented in Fig. 1 (vide supra) and the main aim of this Section was to optimize the rate of the reagent feed into the reactor to provide the plug flow regime and full conversion of precursor. Taking into account the obtained results of kinetic investigations as well as TEM and XRD measurements the optimal conditions

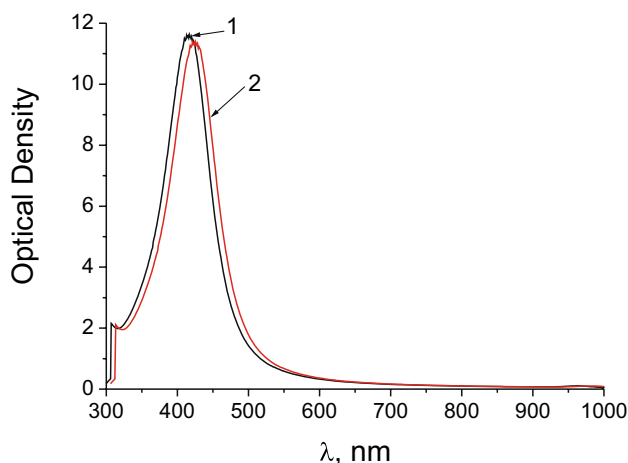
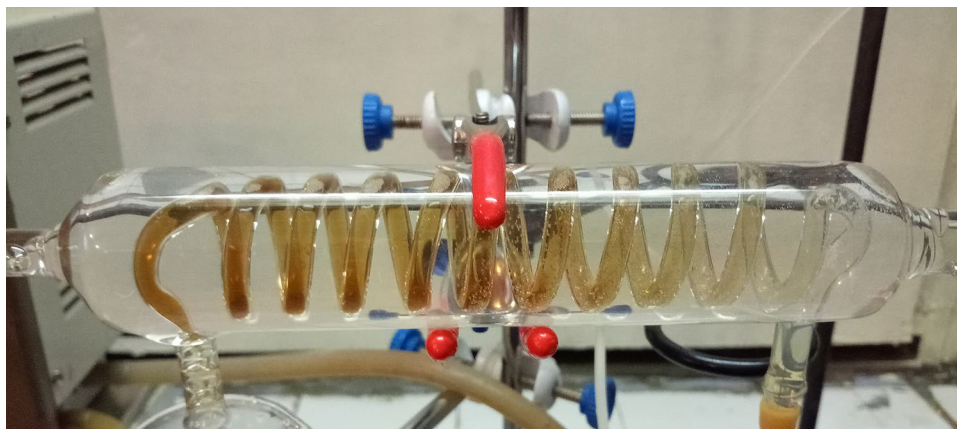


Fig. 10 UV–vis spectra of AgNPs solutions obtained in a batch reactor (1) and in a continuous tubular reactor (2)

Fig. 11 A change of the color of reaction mixture during reaction in a continuous tubular reactor



for the synthesis of AgNPs may be considered as follow: $t = 70\text{ }^\circ\text{C}$, $\text{pH } 10$, $C(\text{RL}) = 4\text{ g/L}$, $[\text{Ag}^+]_0 = 1 \times 10^{-3}\text{ mol/L}$. Such conditions provide a high rate of reaction which is close to the rate of some fast electrochemical processes of AgNPs formation, for example with the rate of microplasma synthesis of AgNPs (Kuntiyi et al. 2021a, b).

The completeness of Ag^+ ions transformation was tested using UV–vis spectroscopy. It was found that in our case the optimal rate of the reagent feed was $\sim 1\text{ mL/min}$ of “ $\text{Ag}^+ + \text{RL}$ ” solution. Such a rate provides the complete conversion of Ag^+ ions into the AgNPs. As we can see from Fig. 10 the UV–vis spectra of AgNPs obtained at the final of the kinetic experiment and AgNPs obtained in the tubular reactor are very close. Such value of the reagent feed rate may be explained as follow. As it can be seen from Fig. 4b, the reaction of reducing Ag^+ ions by RL at above-mentioned conditions have completed at $\sim 10\text{ min}$. Then, it is logical to assume that the rate of the reagent feed is equal to the volume of the reactor divided by the time of the reaction carrying out.

Despite the relatively low rate of the flow of the reaction mixture, the plug flow regime in the reactor was observed (Fig. 11). This fact may be caused by the relatively high value of the flow linear velocity in the reactor ($u = 8\text{ cm/min}$), which is determined by the ratio of the volumetric flow rate (ν) and the tube transverse cross-sectional area (S):

$$u = \nu/S. \quad (9)$$

Needless to say, the constructed laboratory setup is only the prototype. However, we can assume that the presented observation as well as the kinetic experiments may be considered as “the starting point” for the development of industrial reactors for the preparation of the solutions of AgNPs.

Conclusions

The method of “green” synthesis of silver nanoparticles in rhamnolipid solutions is presented. It was found that the average diameter of the obtained AgNPs is 2.6 nm and does not depend on the initial concentration of Ag⁺ but is increased twice with the decrease of the concentration of RL from 4 to 1 g/L. The kinetics of the formation of AgNPs was studied in detail. It was found that both the rate of nucleation and the rate of growth of AgNPs are extremely increased with the increase of pH and temperature. The activation energies of the nucleation and of the growth processes are close and are equal to 135 and 140 kJ/mol, respectively. The kinetic curves of AgNPs formation were fitted using different types of Finke-Watzky schemes. It was found that at the concentration of RL equal to 1 g/L the mechanism of particle formation occurs via the steps of agglomeration subsequent by the autocatalytic growth of formed agglomerates. On the contrary, at the concentration of RL equal to 4 g/L the kinetic curves are well-fitted using the FW-2 scheme. This fact confirms the absence of agglomeration of the particles in the stage of AgNPs growth. The optimal conditions for the production of the solutions “AgNPs-RL” were established as pH 10, temperature 70 °C, C(RL)= 4 g/L and initial concentration of Ag⁺ equal to 0.001 mol/L. A laboratory model of a flow tubular reactor for the synthesis of “AgNPs-RL” colloidal solutions has been created and the optimal flow rate of the reaction solution for providing full transformation of precursors was established.

Supplementary Information The online version contains supplementary material available at <https://doi.org/10.1007/s13204-022-02751-9>.

Acknowledgements This work was carried out with the partial financial support of the National Research Foundation of Ukraine (“Design of polyfunctional nanostructured mono- and bimetallics with electrocatalytic and antimicrobial properties” Agreement 165/02.2020). The authors are grateful to Professor Olena Karpenko and her scientific group from the Department of PhChFF InPOCC NAS of Ukraine for the provided samples of rhamnolipid. The research was partially performed on the equipment of the Scientific Equipment Collective Use Center: “Laboratory of Advanced Technologies, Creation and Physico-Chemical Analysis of New Substances and Functional Materials” (<https://lpnu.ua/ckkno>). Some separated (the motivation of the investigations and short result discussion) results obtained by the authors were partially presented as a poster at the International conference “Nanotechnology and nanomaterials” (NANO-2021) (August 25–27, 2021, Lviv, Ukraine).

Data availability All data generated or analysed during this study are included in this published article.

Declarations

Conflict of interest On behalf of all authors, the corresponding author states that there is no conflict of interest.

References

- Ahmad S, Munir S, Zeb N, Ullah A, Khan B, Ali J, Bilal M, Omer M, Alamzeb M, Salman SM, Ali S (2019) Green nanotechnology: a review on green synthesis of silver nanoparticles—an ecofriendly approach. *Int J Nanomedicine* 14:5087 (10.2147/2FIJN.S200254)
- Akselrud L, Grin Y (2014) WinCSD: software package for crystallographic calculations (Version 4). *J Appl Cryst* 47(2):803–805. <https://doi.org/10.1107/S1600576714001058>
- Amoaghaie R, Saeri MR, Azizi M (2015) Synthesis, characterization and biocompatibility of silver nanoparticles synthesized from *Nigella sativa* leaf extract in comparison with chemical silver nanoparticles. *Ecotoxicol Environ Saf* 120:400–408. <https://doi.org/10.1016/j.ecoenv.2015.06.025>
- Atwater HA, Polman A (2010) Plasmonics for improved photovoltaic devices. *Nat Mater* 9:205–213. https://doi.org/10.1142/9789814317665_0001
- Bar H, Bhui DKR, Sahoo GP, Sarkar P, De SP, Misra A (2009) Green synthesis of silver nanoparticles using latex of *Jatropha curcas*. *Colloids Surf A* 339:134–139. <https://doi.org/10.1016/j.colsurfa.2009.02.008>
- Bazylyak L, Kytsya A, Kuntiyi O, Koretska N, Pokynbroda T, Prokopalo A, Karpenko O (2022) Synthesis and antimicrobial activity of silver nanoparticles stabilized by rhamnolipid. *Visnyk Lviv Univ Ser Chem* 63:363–372. <https://doi.org/10.30970/vch.6301.363>. (In Ukrainian)
- Besson C, Finney EE, Finke RG (2005) Nanocluster nucleation, growth, and then agglomeration kinetic and mechanistic studies: a more general, four-step mechanism involving double autocatalysis. *Chem Mat* 17(20):4925–4938. <https://doi.org/10.1021/cm050207x>
- Bhainsa KC, D’Souza SF (2006) Extracellular biosynthesis of silver nanoparticles using the fungus *Aspergillus fumigatus*. *Colloids Surf B* 47:160–164. <https://doi.org/10.1016/j.colsurfb.2005.11.026>
- Chandran SP, Chaudhary M, Pasricha R, Ahmad A, Sastry M (2006) Synthesis of gold nanotriangles and silver nanoparticles using *Aloe vera* plant extract. *Biotechnol Prog* 22:577–583. <https://doi.org/10.1021/bp050142z>
- Deepak V, Umamaheshwaran PS, Guhan K, Nanthini RA, Krithiga B, Jaithoon NM, Gurunathan S (2011) Synthesis of gold and silver nanoparticles using purified URAK. *Colloid Surface B* 86:353–358. <https://doi.org/10.1016/j.colsurfb.2011.04.019>
- Desireddy A et al (2013) Ultrastable silver nanoparticles. *Nature* 501:399–402. <https://doi.org/10.1038/nature12523>
- Finney EE, Finke RG (2008) The four-step, double-autocatalytic mechanism for transition-metal nanocluster nucleation, growth, and then agglomeration: metal, ligand, concentration, temperature, and solvent dependency studies. *Chem Mat* 20(5):1956–1970. <https://doi.org/10.1021/cm071088j>
- Finney EE, Shields SP, Buhro WE, Finke RG (2012) Gold nanocluster agglomeration kinetic studies: evidence for parallel bimolecular plus autocatalytic agglomeration pathways as a mechanism-based alternative to an avrami-based analysis. *Chem Mater* 24(10):1718–1725. <https://doi.org/10.1021/cm203186y>
- Grytsenko O, Pokhmurska A, Suberliak S, Kushnirchuk M, Panas M, Moravskiy V, Kovalchuk R (2018) Technological features in obtaining highly effective hydrogel dressings for medical purposes. *East Eur J Enterp Technol* 6(6):6–13. <https://doi.org/10.15587/1729-4061.2018.150690>
- Gurunathan S, Kalishwaralal K, Vaidyanathan R, Deepak V, Pandian SRK, Muniyandi J, Hariharan N, Eom SH (2009) Biosynthesis, purification and characterization of silver nanoparticles using

- Escherichia coli*. Colloids Surf B 74:328–335. <https://doi.org/10.1016/j.colsurfb.2009.07.048>
- Gurunathan S, Han J, Park JH, Kim JH (2014a) A green chemistry approach for synthesizing biocompatible gold nanoparticles. Nanoscale Res Lett 9:248. <https://doi.org/10.1186/1556-276X-9-248>
- Gurunathan S, Han JW, Kwon DN, Kim JH (2014b) Enhanced antibacterial and anti-biofilm activities of silver nanoparticles against Gram-negative and Gram-positive bacteria. Nanoscale Res Lett 9:373. <https://doi.org/10.1186/1556-276X-9-373>
- Gurunathan S, Jeong JK, Han JW, Zhang XF, Park JH, Kim JH (2015) Multidimensional effects of biologically synthesized silver nanoparticles in *Helicobacter pylori*, *Helicobacter felis*, and human lung (L132) and lung carcinoma A549 cells. Nanoscale Res Lett 10:1–17. <https://doi.org/10.1186/s11671-015-0747-0>
- Gurunathan S (2015) Biologically synthesized silver nanoparticles enhances antibiotic activity against Gram-negative bacteria. J Ind Eng Chem 29:217–226. <https://doi.org/10.1016/j.jiec.2015.04.005>
- Hoops S, Sahle S, Gauges R, Lee C, Pahle J, Simus N, Singhal M, Xu L, Mendes P, Kummer U (2006) COPASI—a CComplex Pathway Simulator. Bioinformatics 22(24):3067–3074. <https://doi.org/10.1093/bioinformatics/btl485>
- Kalimuthu K, Babu RS, Venkataraman D, Bilal M, Gurunathan S (2008) Biosynthesis of silver nanocrystals by *Bacillus licheniformis*. Colloid Surface B 65:150–153. <https://doi.org/10.1016/j.colsurfb.2008.02.018>
- Kalishwaralal K, Deepak V, RamKumarPandian S, Nellaiah H, Sangiliyandi S (2008) Extracellular biosynthesis of silver nanoparticles by the culture supernatant of *Bacillus licheniformis*. Mater Lett 62:4411–4413. <https://doi.org/10.1016/j.matlet.2008.06.051>
- Kalishwaralal K, Deepak V, RamKumarPandian S, Kottaisamy M, BarathManiKanth S, Kartikeyan B, Gurunathan S (2010) Biosynthesis of silver and gold nanoparticles using *Brevibacterium casei*. Colloids Surf B 77:257–262. <https://doi.org/10.1016/j.colsurfb.2010.02.007>
- Kapoor RT, Salvadori MR, Rafatullah M, Siddiqui MR, Khan MA, Alshareef SA (2021) Exploration of microbial factories for synthesis of nanoparticles—a sustainable approach for bioremediation of environmental contaminants. Front Microbiol 12:1404. <https://doi.org/10.3389/fmicb.2021.658294>
- Karpenko EV, Pokynbroda TY, Makitra RG, Palchikova EY (2009) Optimal methods for isolating the biogenic surfactant rhamnolipids. J Gen Chem 12:2011 (in Russian)
- Klaus T, Joerger R, Olsson E, Granqvist CG (1999) Silver-based crystalline nanoparticles, microbially fabricated. Proc Natl Acad Sci USA 96:13611–13614. <https://doi.org/10.1073/pnas.96.24.13611>
- Koval'chuk EP, Ogenko VM, Reshetnyak OV, Pereviznyk OB, Davydenko N, Marchuk IE (2010) Surface modification of silver microparticles with 4-thioaniline. Electrochimica Acta 55(18):5154–5162. <https://doi.org/10.1016/j.electacta.2010.04.023>
- Krishnaraj C, Jagan EG, Rajasekar S, Selvakumar P, Kalaichelvan PT, Mohan N (2010) Synthesis of silver nanoparticles using *Acalypha indica* leaf extracts and its antibacterial activity against water borne pathogens. Colloids Surf B 76:50–56. <https://doi.org/10.1016/j.colsurfb.2009.10.008>
- Kumar A, Vemula PK, Ajayan PM, John G (2008) Silver nanoparticle embedded antimicrobial paints based on vegetable oil. Nat Mater 7:236–241. <https://doi.org/10.1038/nmat2099>
- Kumar B, Smita K, Cumbal L, Debut A, Pathak RN (2014) Sonochemical synthesis of silver nanoparticles using starch: a comparison. Bioinorg Chem Appl 2014:784268. <https://doi.org/10.1155/2014/784268>
- Kuntyi OI, Kytsya AR, Bondarenko AB, Mazur AS, Mertsalo IP, Bazylyak LI (2021a) Microplasma synthesis of silver nanoparticles in PVP solutions using sacrificial silver anodes. Colloid Polymer Sci 299(5):855–863. <https://doi.org/10.1007/s00396-021-04811-y>
- Kuntyi O, Mazur A, Kytsya A, Karpenko O, Bazylyak L, Mertsalo I, Pokynbroda T, Prokopalo A (2020) Electrochemical synthesis of silver nanoparticles in solutions of rhamnolipid. Micro Nano Lett 15(12):802–807. <https://doi.org/10.1049/mnl.2020.0195>
- Kuntyi O, Zozulya G, Kytsya A (2021b) “Green” synthesis of metallic nanoparticles by sonoelectrochemical and sonogalvanic replacement methods. Bioinorg Chem Appl 2021:9830644. <https://doi.org/10.1155/2021/9830644>
- Kytsya A, Bazylyak L, Simon P, Zelenina I, Antonyshyn I (2019) Kinetics of Ag300 nanoclusters formation: the catalytically effective nucleus via a steady-state approach. Int J Chem Kinet 51(4):266–273. <https://doi.org/10.1002/kin.21249>
- Kytsya AR, Reshetnyak OV, Bazylyak LI, Hrynda YM (2014) UV/VIS-spectra of silver nanoparticles as characteristics of their sizes and sizes distribution. In: Zaikov GE, Bazylyak LI, Haghi AK (eds) Functional polymer blends and nanocomposites: a practical engineering approach, 1st edn. Apple Academic Press, New York, pp 231–239. <https://doi.org/10.1201/b16895>
- Leung TC, Wong CK, Xie Y (2010) Green synthesis of silver nanoparticles using biopolymers, carboxymethylated-curdlan and fucoidan. Mater Chem Phys 121:402–405. <https://doi.org/10.1016/j.matchemphys.2010.02.026>
- Lee SH, Jun BH (2019) Silver nanoparticles: synthesis and application for nanomedicine. Int J Mol Sci 20(4):865. <https://doi.org/10.3390/ijms20040865>
- Mousavi SM, Hashemi SA, Ghasemi Y, Atapour A, Amani AM, Savar-Dashtaki A, Babapoor A, Arjmand O (2018) Green synthesis of silver nanoparticles toward bio and medical applications: review study. Artif Cells Nanomed Biotechnol 46(p3):S855–S872. <https://doi.org/10.1080/21691401.2018.1517769>
- Nair B, Pradeep T (2002) Coalescence of nanoclusters and formation of submicron crystallites assisted by Lactobacillus strains. Cryst Growth Des 2:293–298. <https://doi.org/10.1021/cg0255164>
- Nanda A, Saravanan M (2009) Biosynthesis of silver nanoparticles from *Staphylococcus aureus* and its antimicrobial activity against MRSA and MRSE. Nanomed Nanotechnol 5:452–456. <https://doi.org/10.1016/j.nano.2009.01.012>
- Özkar S, Finke RG (2016) Palladium(0) nanoparticle formation, stabilization, and mechanistic studies: Pd(acac)₂ as a preferred precursor. [Bu₄N] 2HPO₄ stabilizer, plus the stoichiometry, kinetics, and minimal, four-step mechanism of the palladium nanoparticle formation and subsequent agglomeration reactions. Langmuir 32(15):3699–3716. <https://doi.org/10.1021/acs.langmuir.6b00013>
- Plaža G, Chojniak J, Mendrek B, Trzebicka B, Kvitěk L, Panacek A, Prucek R, Zboril R, Paraszkievicz K, Bernat P (2016) Synthesis of silver nanoparticles by *Bacillus subtilis* T-1 growing on agro-industrial wastes and producing biosurfactant. IET Nanobiotechnol 10:62–68. <https://doi.org/10.1049/iet-nbt.2015.0016>
- Pokynbroda TY, Karpenko IV, Mityana HH, Karpenko OY (2019) Isolation of surfactants synthesized by the pseudomonas bacteria and study of their properties. Innov Biosys Bioeng 3(2):70–76. <https://doi.org/10.20535/ibb.2019.3.2.165838>
- Sandoe HE, Watzky MA, Diaz SA (2019) Experimental probes of silver metal nanoparticle formation kinetics: comparing indirect versus more direct methods. Int J Chem Kinet 51:861–871. <https://doi.org/10.1002/kin.21315>
- Shahverdi AR, Minaeian S, Shahverdi HR, Jamalifar H, Nohi AA (2007) Rapid synthesis of silver nanoparticles using culture supernatants of Enterobacteria: a novel biological approach. Process Biochem 42:919–923. <https://doi.org/10.1016/j.procbio.2007.02.005>
- Shankar S, Rhim JW (2015) Amino acid mediated synthesis of silver nanoparticles and preparation of antimicrobial agar/silver

- nanoparticles composite films. *Carbohydr Polym* 130:353–363. <https://doi.org/10.1016/j.carbpol.2015.05.018>
- Slistan-Grijalva A, Herrera-Urbina R, Rivas-Silva JF, Ávalos-Borja M, Castellón-Barraza FF, Posada-Amarillas A (2005) Classical theoretical characterization of the surface plasmon absorption band for silver spherical nanoparticles suspended in water and ethylene glycol. *Phys E* 27:104–112. <https://doi.org/10.1016/j.physe.2004.10.014>
- Some S, Sen IK, Mandal A, Aslan T, Ustun Y, Yilmaz EŞ, Kati A, Demirbas A, Mandal AK, Ocsay I (2018) Biosynthesis of silver nanoparticles and their versatile antimicrobial properties. *Mater Res Express* 6(1):012001. <https://doi.org/10.1088/2053-1591/aae23e>
- Srikar SK, Giri DD, Pal DB, Mishra PK, Upadhyay SN (2016) Green synthesis of silver nanoparticles: a review. *Green Sustain Chem* 6(1):34–56. <https://doi.org/10.4236/gsc.2016.61004>
- Sun Y, Xia Y (2002) Shape-controlled synthesis of gold and silver nanoparticles. *Science* 298:2176–2179. <https://doi.org/10.1126/science.1077229>
- Syafiuddin A, Salmiati Salim MR, Kueh ABH, Hadibarata T, Nur HA (2017) Review of silver nanoparticles: research trends, global consumption, synthesis, properties, and future Challenges. *J Clin Chem Soc* 64:732–756. <https://doi.org/10.1002/jccs.201700067>
- Vigneshwaran N, Ashtaputre NM, Varadarajan PV, Nachane RP, Paralikar KM, Balasubramanya RH (2007) Biological synthesis of silver nanoparticles using the fungus *Aspergillus flavus*. *Mater Lett* 61:1413–1418. <https://doi.org/10.1016/j.matlet.2006.07.042>
- Vilchis-Nestor AR, Sanchez-Mendieta V, Camacho-Lopez MA, Gomez-Espinosa RM, Camacho-Lopez MA, Arenas-Alatorre JA (2008) Solventless synthesis and optical properties of Au and Ag nanoparticles using *Camellia sinensis* extract. *Mater Lett* 62:3103–3105. <https://doi.org/10.1016/j.matlet.2008.01.138>
- Watzky MA, Finke RG (1997) Transition metal nanocluster formation kinetic and mechanistic studies. A new mechanism when hydrogen is the reductant: slow, continuous nucleation and fast autocatalytic surface growth. *J Am Chem Soc* 119(43):10382–10400. <https://doi.org/10.1021/ja9705102>
- Widegren JA, Aiken JD, Özkar S, Finke RG (2001) Additional investigations of a new kinetic method to follow transition-metal nanocluster formation, including the discovery of heterolytic hydrogen activation in nanocluster nucleation reactions. *Chem Mater* 13(2):312–324. <https://doi.org/10.1021/cm0006852>
- Yerokhin V, Pokynbroda T, Karpenko O, Novikov V (2006) Study of the growth and synthesis of the target product by the strain *Pseudomonas* species PS-17—producer of extracellular biosurfactants. *Visn Natsion Univrs “Lvivska Politehnika”* 553:124–127 (in Ukrainian)

Publisher's Note Springer Nature remains neutral with regard to jurisdictional claims in published maps and institutional affiliations.

Springer Nature or its licensor (e.g. a society or other partner) holds exclusive rights to this article under a publishing agreement with the author(s) or other rightsholder(s); author self-archiving of the accepted manuscript version of this article is solely governed by the terms of such publishing agreement and applicable law.